UCRL-JC-131189
PREPRINT

Identification of Mine Collapses, Explosions and Earthquakes Using INSAR: A Preliminary Investigation

W. Foxall
J.J. Sweeney
W.R. Walter

This paper was prepared for submittal to the
20th Seismic Research Symposium
Santa Fe, NM
September 21-23, 1998

July 7, 1998

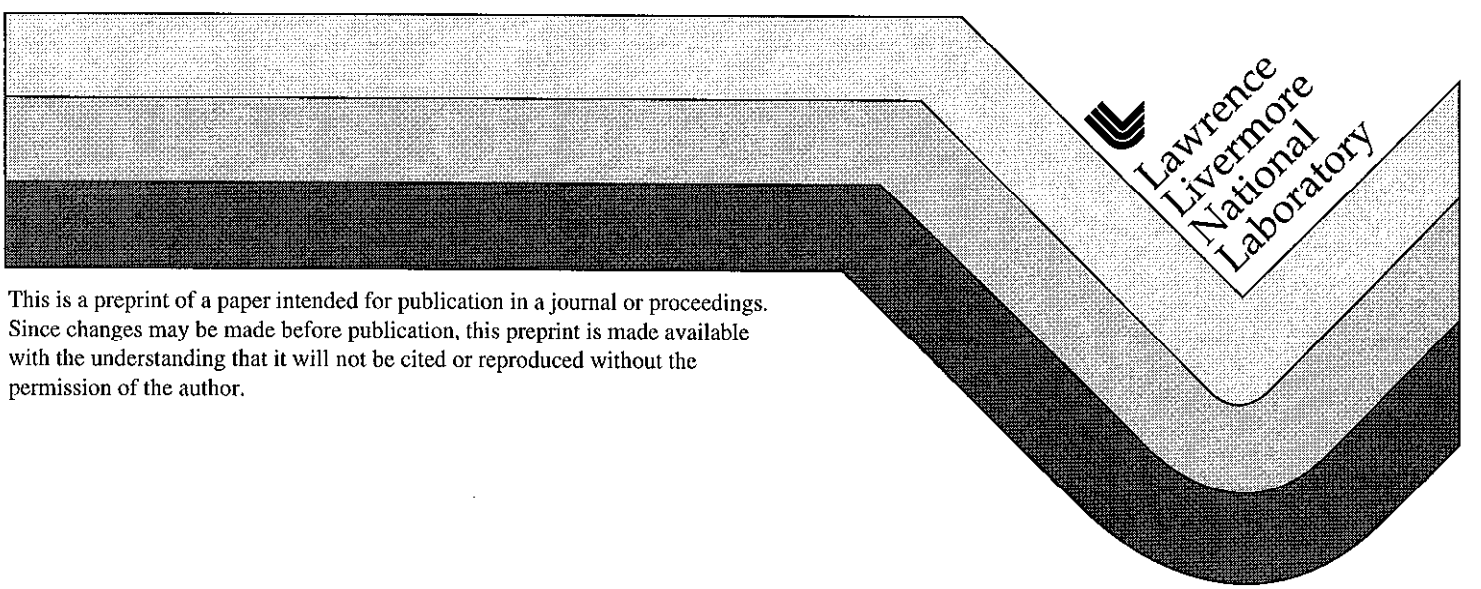

IDENTIFICATION OF MINE COLLAPSES, EXPLOSIONS AND EARTHQUAKES USING INSAR: A PRELIMINARY INVESTIGATION

Bill Foxall, Jerry J. Sweeney, William R. Walter

Lawrence Livermore National Laboratory, P.O. Box 808, Livermore California

Contract No. W-7405-ENG-48.
Sponsored by U.S. Department of Energy
Office of Nonproliferation and National Security
Office of Research and Development

ABSTRACT

Interferograms constructed from satellite-borne synthetic aperture radar images have the capability of mapping sub-cm ground surface deformation over areas on the order of 100 x 100 km with a spatial resolution on the order of 10 meters. We investigate the utility of synthetic aperture radar interferometry (InSAR) used in conjunction with regional seismic methods in detecting and discriminating different types of seismic events in the context of special event analysis for the CTBT. For this initial study, we carried out elastic dislocation modeling of underground explosions, mine collapses and small ($M<5.5$) shallow earthquakes to produce synthetic interferograms and then analyzed satellite radar data for a large mine collapse. The synthetic modeling shows that, for a given magnitude each type of event produces a distinctive pattern of ground deformation that can be recognized in, and recovered from, the corresponding interferogram. These diagnostic characteristics include not only differences in the polarities of surface displacements but also differences in displacement amplitudes from the different sources. The technique is especially sensitive to source depth, a parameter that is crucial in discriminating earthquakes from the other event types but is often very poorly constrained by regional seismic data alone.

The ERS radar data analyzed is from a M_L 5.2 seismic event that occurred in southwestern Wyoming on February 3, 1995. Although seismic data from the event have some characteristics of an underground explosion, based on seismological and geodetic data it has been identified as being caused by a large underground collapse in the Solvay Mine. Several pairs of before-collapse and after-collapse radar images were phase processed to obtain interferograms. The minimum time separation for a before-collapse and after-collapse pair was 548 days. Even with this long time separation, phase coherence between the image pairs was acceptable and a deformation map was successfully obtained. Two images, separated by 1 day and occurring after the mine collapse, were used to form a digital elevation map (DEM) that was used to correct for topography. The interferograms identify the large deformation at the Solvay Mine as well as some areas of lesser deformation near other mines in the area. The large amount of deformation at the Solvay Mine was identified, but (as predicted by our dislocation modeling) could not be quantified absolutely because of the incoherent interference pattern it produced

Key Words: Radar interferometry, synthetic aperture radar, discrimination, seismology, surface deformation, treaty monitoring

This work was performed under the auspices of the U.S. Department of Energy by Lawrence Livermore National Laboratory under contract No. W-7405-Eng-48 for the Office of Research and Development, NN-20, within the Office of NonProliferation and National Security, NN-1.

Introduction

Synthetic aperture radar interferometry (InSAR) using commercially available images from satellite-borne radars is rapidly finding a wide variety of earth science applications. The four platforms currently in orbit, the European ERS-1 and ERS-2, Japanese JERS and Canadian RADARSAT satellites, provide broad coverage of the Earth's surface. The technique is capable of mapping ground surface deformation at sub-centimeter accuracy over an area on the order of 100x100 km and with a spatial resolution on the order of 10m. In this paper we evaluate the potential of InSAR used in conjunction with regional seismic analysis to detect, characterizing and discriminate the different types of seismic events that potentially may trigger a Comprehensive Test Ban Treaty (CTBT) alert. The three types of events we consider are underground explosions, shallow earthquakes and sudden mine collapses. We focus on events having magnitudes of 5.5 and below. Regional seismic analysis generally provides moderate constraint on the epicenters and sizes of these small events, but often the constraint on their focal depths and mechanisms is insufficient to enable the event to be characterized reliably. In particular, some of the seismological features produced by mine collapses are similar to those associated with explosions. However, the depth and mechanism of the source are the parameters that strongly control the amplitude and pattern of surface static deformation. Therefore, given the approximate location of an event, we can take advantage of the very broad coverage provided by satellite-borne SAR together with its remarkable accuracy and resolution to examine the surface deformation pattern produced by the event, and hence place bounds on its depth and mechanism.

The first part of our investigation involves elastic dislocation modeling of the different source types to generate synthetic interferograms. In this modeling we evaluate the detection and diagnostic capabilities of InSAR by examining systematically the differences among the ground deformation signatures of the different sources and the tradeoffs among the source parameters. The ultimate objective of the modeling work is to develop a search procedure to constrain bounds on source parameters using interferograms. In this paper, we present examples of synthetic interferograms and the corresponding ground deformation fields to demonstrate the potential of the technique, and show the sensitivity of the ground deformation to variations in specific parameters. We then present the results of an analysis of SAR data for a large (M_L 5.2) mine collapse. This event has been the subject of seismological and geodetic studies, as well as extensive investigations within the mine itself. We obtained several SAR images of the region surrounding the mine, and, despite the fact that the available data coverage is less than optimal, it was possible to construct an interferogram of relatively high quality and to derive a clear surface deformation map. Interpretation of the interferogram and deformation map illustrates the power and utility of InSAR, as well as highlighting one of its chief limitations for investigating shallow, large-displacement events. The area of large surface deformation associated with the collapse is clearly seen, as well as extensive areas of lesser deformation, which we interpret to be continuous subsidence caused by ground water withdrawal and by routine mining operations.

InSAR Methodology

In this section we provide a brief overview of InSAR methodology. An in-depth treatment of the theory of InSAR and its application to ground deformation mapping is given in Zebker et al. (1994). The geometry of the InSAR problem is shown in Figure 1. P_1 and P_2 are the orbital positions of the SAR satellite during two different passes and R_1 and R_2 the corresponding slant ranges to a target on the Earth's surface for the look-angle, θ. The distance between the satellite positions is the baseline, B. The SAR data consist of complex (i.e. amplitude and phase) radar images backscattered from very large areas ("scenes") of the Earth's surface, typically on the order of 100x100 km. Each image is composed of a mosaic of resolution elements, or pixels, having dimensions of about 10-20m. In the image obtained from each pass of the satellite the phase of the backscattered signal from each pixel is proportional to the two-way path length from the radar to the pixel plus the sum of the random phases from the scattering elements within the pixel. Assuming that the scattering within each pixel is the same for the images obtained from two close-by passes, differencing the phases, pixel by pixel, of those images cancels the random component of the phase, leaving only the phase difference corresponding to the difference between the path lengths to the two satellite positions. Baseline lengths of a few hundred meters or less are optimal. The resulting interferogram maps the range-related phase differences over the entire scene. Differences in range that are correlated over many pixels appear as coherent fringes of constant phase difference, like those shown in Figure 2.

The path length differences mapped by an interferogram contain contributions from the topography and from any ground surface displacement that occurs at a scale larger than the pixel size during the interval between the two satellite passes. Therefore, to recover the ground displacement the topographic contribution must be removed from

the interferogram. This is done either using an existing digital elevation model (DEM) for the area covered by the scene (e.g. Massonet et al., 1993) or by deriving the DEM directly by "double differencing" two interferograms made from three or more images of the same scene (e.g. Zebker et al., 1994). Each fringe in the interferogram represents motion in the range direction of one-half of the radar wavelength, i.e. about 2.8 cm for C-band (ERS-1, ERS-2, RADARSAT) and 13 cm for L-band (JERS). The phase differences are measured modulo 2π, so that the interferogram must be phase- unwrapped to recover the surface displacement. This is achieved by starting at points on the interferogram where the displacement is assumed to be zero, and adding half-wavelength increments of displacement for every complete fringe crossed. This enables a precision on the order of one-tenth of a radar wavelength to be achieved.

The main sources of error in InSAR are atmospheric water vapor, which can introduce spurious path length differences, and the high fringe rates associated with steep topography. Since concentrations of water vapor are short-lived, these spurious signals can be identified by using two or more pairs of images obtained at different times. The main limitation in the method comes from deformation at sub-pixel scale or changes in surface reflectivity, which destroys the phase coherence between the images used to form the interferogram. This is caused, for example, by vegetation growth or reworking of the ground surface. In general, the method is best suited to arid regions with moderate topography. The decorrelation effects are cumulative with time and are therefore minimized by choosing pairs of images that are as close together in time as possible. Steep displacement gradients that correspond to fringe spacings approaching the width of a pixel or less also result in loss of correlation. This limitation is particularly acute when dealing with large displacements such as those produced by some of the shallow events considered in the present application.

Forward Modeling

In this section we compare the characteristics of the surface deformation signatures and corresponding interferograms generated by models of underground explosions, mine collapses and shallow earthquakes in an elastic medium, and demonstrate the sensitivity of the deformation patterns to variations in selected source parameters. We consider events having magnitudes less than m_b5.5. Moderately reliable epicenter and magnitude estimates are normally available for events of this size from seismic analysis, but source depths and mechanisms are often poorly determined. We model the surface deformation fields using the Green's functions of Okada (1985) for dislocation sources in an homogeneous, semi-infinite elastic half space. Explosive and earthquake sources are modeled as dilatational and rectangular shear dislocations, respectively. Mine collapses are modeled as closing horizontal tensile cracks. This representation has been shown by Pechmann et al. (1995) to provide a satisfactory fit to far-field waveform data recorded from the 1995 Solvay mine collapse event discussed below. While elastic modeling generally provides satisfactory fits to earthquake deformation data (e.g. Feigl et al., 1995), it is expected to give only a general idea of some of the main features of the deformation fields produced by explosions detonated in weak near-surface materials. However the objective of this preliminary study is to compare the first-order characteristics of the deformation fields and interferograms produced by the different sources.

To facilitate comparisons among the event types, we assume that we have a magnitude estimate from seismic analysis, and select the source parameters of each of the event types within realistic bounds to match the moment corresponding to that magnitude. Source areas and closing displacements for collapse events are within the range of typical dimensions of mine workings. Earthquake source areas and displacements are based on empirical data and are constrained to produce stress drops of 10-200 bars, the range conventionally assumed for small earthquakes. Source depths are restricted to the normal range expected for each event type, 0.1-1 km for underground explosions, 0.3-2 km for collapse events, and greater than 2 km for earthquakes. The deformation fields are sampled on a 20x20m grid to simulate the spatial resolution of SAR.

Figure 2 compares the surface deformation fields for events having a magnitude of about m_b5.0. This corresponds to a seismic moment of 3.0×10^{16} Nm for earthquakes and mine collapses, and a dipole moment of 1.4×10^{15} Nm for explosions (Patton and Walter, 1993, 1994). m_b5.0 corresponds to an explosive yield of approximately 20 kT for a well-coupled event (Murphy, 1996). The mine collapse is modeled as a 1x1 km source area with a closing displacement of 1m. The earthquake is modeled as 0.4m of pure dip slip displacement over a 1.6x1.6 km fault that strikes N and dips 30°E. The surface projections of the collapse and earthquake sources are shown on Figure 2. The shallow (2 km) focal depth of the earthquake is assumed to be near the minimum for events of this size. The elastic half space used for all the event types has a Poisson ratio of 0.25 and a rigidity of

$3x10^{10}$Nm. The deformation fields are resolved into the range direction of a radar in a polar orbit with a look-angle of 23° , similar to that of ERS-1 and -2. One fringe on the interferograms in Figure 2 corresponds to a change in radar range of 2.8 cm.

Each of the surface deformation fields shown in Figure 2 has distinctive features that are characteristic of the corresponding source type. The first and most striking difference among the events is the much smaller area of the surface deformation produced by the explosion, despite its shallow source depth. This is due to the much smaller moment of the explosive source in relation to the specified magnitude, compared with the other source types. In this elastic calculation, the explosion produces a maximum displacement of about 3 cm, corresponding to a single fringe in the interferogram. The second distinguishing feature of the explosion signal, of course, is its upward displacement polarity (decrease in radar range), opposite to that of the collapse and normal faulting events (dilatation in the hanging wall of this shallow-dipping normal fault is well below the InSAR detection threshold). The main characteristic that differentiates the mine collapse from the other events is its much greater deformation amplitude. The collapse generates a maximum displacement of 30 cm and an interferogram with eleven fringes, while the maximum displacement from the earthquake is approximately 5 cm (two fringes). Since the collapse and earthquake signatures are roughly the same width, the displacement gradient, and hence the fringe rate, above the collapse are also much greater than those above the earthquake. It is important to note that the large differences between the earthquake interferogram and those of the other sources are obtained even though the exceptionally shallow focal depth of the earthquake maximizes the surface deformation it produces. In general, these differences result from the way the moment is realized in each source; the relatively large closing displacement of a typical mine collapse is concentrated in a small area, whereas, to achieve the same moment, the smaller shear displacement of an earthquake is distributed over a larger fault area.

The earthquake and collapse interferograms shown in Figure 3 were calculated by simulating real events for which source parameters are available. The first is a Dec. 4, 1992 M_w5.1 aftershock of the Landers earthquake and the second the 1995 M_L5.2 collapse at the Solvay mine in Wyoming (Pechmann et al., 1995), which is described in the next section. The earthquake was located at a depth of 2.6 km (Feigl et al., 1995), and the mine collapse occurred at a depth of 500m (U.S. Mine Safety and Health Administration [MSHA] 1996). The Landers aftershock is modeled as 0.5m of right-reverse (rake 93°) displacement on a 3.1 x 2.9 km fault plane dipping 28° (Feigl et al., 1995). Based on observations in the MSHA report, the Solvay collapse is modeled as the closing of a cavity 2x1 km in area and 1.3m high. The simulated explosion has a magnitude of m_b5.2 and a depth of 0.3 km. The simulated interferograms for these events shown in Figure 3 each have the same general characteristics as seen in Figure 2. The explosion and earthquake interferograms have clearly defined fringes, and the latter closely matches the actual interferogram reported by Massonet et al. (1993) for the Landers aftershock. However, the differential phase in the collapse interferogram is incoherent except for the outer one or two fringes. This illustrates one of the chief limitations in using InSAR to analyze shallow, large-displacement, concentrated sources. The maximum displacement over the collapse event is about 0.9m, which results in a displacement gradient on the order of 1m/km. This corresponds to a fringe spacing of about 30m, approaching the 20m pixel size, so the interferogram essentially is spatially aliased.

Figure 4 shows the displacement fields for m_b5 events for various source depths calculated using the source parameters and elastic constants as used for Figure 3. The horizontal dashed line on Figure 4 shows the displacement threshold (2.8 cm) corresponding to one C-band interference fringe. Theoretically, a mine collapse of this size (1m closing displacement over a 1x1 km area) at any depth within the range 0.5-2 km is detectable by InSAR, but m_b5 earthquakes having focal depths greater than about 3 km will not be detected. According to these elastic calculations, explosions of this size (10-20 kT) will not be detected if their source depths are greater than about 350m in this stiff medium. However, the displacement amplitudes generated by an explosion are sensitive to the elastic properties of the medium, being significantly greater in the typically softer near-surface materials within which they are detonated. Figure 5 shows the effect on the surface displacement of locating an explosion in a material having elastic properties more typical of the near-surface. The upper curve in Figure 5 was calculated using a Poisson ratio of 0.26 and a rigidity of $1.32x10^{10}$ Nm, which are the values estimated for the shallow subsurface in central Wyoming by Pechmann et al. (1995). Non of the calculations include the inelastic and non-linear effects, such as spall, that are typically observed for subsurface explosions, and which can profoundly influence the characteristics of the surface deformation, nor do they consider cavity collapse. It should be noted, however, that the characteristically narrow width of the surface deformation field that results from all of the elastic calculations (Figures 4 and 5) is likely to remain diagnostic of explosive sources.

SAR Data Analysis for the February 3, 1995 Solvay Mine Collapse

A catastrophic M_L5.1 collapse of part of the Solvay mine in Wyoming occurred on February 3, 1995. Seismic analysis by Pechmann et al. (1995) correctly identified this event as a likely mine collapse. The epicenter was moderately well determined by regional seismic data and is 4.3 km NW of the center of the collapsed part of the mine. The depth was constrained only to be shallower than 10 km. First motion data could be explained equally well by an implosional or normal faulting mechanisms, but the 20-40s waveform data are fit better by the tensile crack collapse source than by any earthquake mechanism. Geodetic surveying after the event revealed surface subsidence up to 0.9m over an area of about 1x2 km corresponding to the collapsed portion of the mine.

We acquired SAR images of the region surrounding the Solvay mine from seven passes of the ERS-1 and -2 satellites. From these we were able to form four pairs of images having short baselines (<200m) that permit interferometry. Three pairs bracket the Solvay collapse event, but the time intervals spanned by these pairs, 548, 688 and 758 days, are relatively long. This is because the ERS-1 satellite was operated over the area of interest in a mode unsuitable for interferometry during the period Dec., 1993-Mar., 1995, so that the latest before-collapse images available are from 1993. The three pairs of images were processed to form interferograms, and the 548-day (Oct. 8, 1993-Apr. 9, 1995) interferogram was selected for further analysis. The data processing was carried out by Atlantis Scientific, Inc. Despite the long time interval, the coherence between the images is good, reflecting the arid environment. The interferogram produced form the fourth pair of images was used to create an accurate DEM. This pair spans one day, and combines ERS-1 and ERS-2 images from a period in 1995 when the two satellites were operated in tandem mode, which provided one-day repeat coverage of most of the Earth's surface. The DEM was used to subtract the topographic phase from the 548-day interferogram to generate the final displacement interferogram. Figure 6 shows the 45x33 km portion of the 110x100 km interferogram covering the region containing the Solvay mine. Figure 6 shows the deformation map created by phase-unwrapping the interferogram. Approximate maximum displacements are shown for various areas.

Although difficult to see on this gray-scale figure, a distinct fringe pattern in the vicinity of the Solvay mine is discernible on Figure 6. Numerous other large- and small-scale fringe patterns can also be seen further to the north. All of these patterns are typical of surface deformation phase signatures, and, since the same patterns appear on the 758-day interferogram it is highly unlikely that they are caused by atmospheric effects. The interference pattern at Solvay consists of slightly more than one complete fringe, corresponding to about 4 cm of subsidence, enclosing an area of about 3.5 km N-S by 3 km E-W centered on the collapsed portion of the mine. Within the area defined by the outer fringe the phase is incoherent, suggesting large surface deformation. The incoherent area is blacked out in the deformation map (Figure 7). The synthetic interferogram modeled for the Solvay collapse shown in Figure 3c is similar to the observed interference pattern, although two coherent fringes can be seen in the (noise-free) synthetic.

Given the approximate source location and size from the seismic analysis, but assuming no prior knowledge of the mine collapse, interpretation of the interferogram permits us to infer: (1) The location of the event; (2) that the event caused surface subsidence and is therefore an earthquake, or involved some form of collapse or volume contraction; (3) an upper bound estimate on the source dimensions, given by the geometry of the first interference fringe; (4) a lower bound estimate on the surface displacement gradient of approximately 1m/km, giving a lower bound on the source displacement of about 1m; (5) given the event size and bounds on the source area and displacement, that this event is not an earthquake. Presumably the event vicinity would also be a known area of active mining. The phase incoherence directly above the collapse is unquestionably due in large part to the large surface deformation. However, the collapse apparently caused a tailings pond above part of the collapse to drain, and surface disruption at sub-pixel scale caused by the collapse and mining-related ground reworking may also have been a contributing factors.

North of the Solvay mine the interferogram indicates three general areas of subsidence. The interference fringes in these areas appear, in general, to be moderately coherent, and Figure 7 shows that the deformation amplitudes are relatively small. The small (1 km^2) area of subsidence immediately to the north of the mine collapse has a maximum amplitude of about 9 cm, and is located above the NW part of the Solvay mine. Within the large, E-W elongated region in the center of Figure 6 numerous small-scale areas of subsidence are superimposed upon the overall wide-scale deformation signature. The subsidence in this area also reaches a maximum of about 9 cm. Subsidence in the broad-scale area of subsidence further to the NNW reaches a maximum of 11 cm. These broad

areas of relatively small, but readily apparent, deformation are typical of subsidence caused by ground-ground water withdrawal, and the smaller-scale deformation centers are similar to those over oil fields. Therefore, it appears that they represent the accumulation of continuous subsidence over the one and a half years spanned by the image pair. Preliminary analysis of interferograms for periods before and after the Feb. 3 collapse indicate that this is the case. The deformation rates estimated from these ongoing studies will be applied to the 548-day interferogram to remove the continuous deformation signal and enhance the collapse signature. It is feasible that, without prior information, the Solvay interference pattern could have been attributed to continuous deformation. Creating interferograms before and after the event will eliminate that possibility.

Discussion and Conclusions

The remarkable areal coverage, spatial resolution and displacement sensitivity provided by InSAR makes it a powerful tool for mapping and analyzing surface deformation resulting from a wide range of subsurface processes. We have evaluated the potential for using InSAR in conjunction with seismological analysis to detect and characterize three types of small ($M<5.5$) seismic events, explosions, mine collapses and earthquakes, that are of interest in CTBT monitoring, but for which seismic analysis alone often provides incomplete information. The results of this preliminary study indicate that given the magnitude and approximate epicenter of an event from seismic analysis, InSAR can under favorable conditions be used to identify the source type and determine bounds on the source parameters and depth.

The elastic modeling results show that each of the event types produces a characteristic interference pattern, and places bounds on the maximum source depth for which an event of a given size can theoretically be detected. Under observational conditions that permit an interferogram with adequate differential phase coherence to be created, these characteristic fringe patterns can be used to accurately locate the event and to discriminate the event type. Source parameters can then be estimated by fitting models to the displacement field obtained by phase-unwrapping the interferogram. In cases where the surface displacements are so large that the interference pattern is incoherent, bounds on source area and displacement can still be estimated. For example, presented with the collapse interferograms shown in Figures 3c and 6, without prior knowledge of the source, we would be able to say that they were produced by large-displacement, shallow events other than earthquakes, and from the area and polarity of the displacement field would be able to identify the sources as collapses. The outer, coherent fringes give the upper bound on the source area and we can place a lower bound on the displacement. These bounds can then be used as constraints in further seismic waveform modeling to refine the source parameters.

The interferogram for the Solvay mine collapse shows that adequate differential phase coherence can be obtained under favorable environmental conditions even when the SAR image pair spans time intervals as great as 1-2 years. Based on this interferogram, the characteristics of the fringe patterns produced by mine collapses and shallow earthquakes should be readily discernible. The interferometric signatures produced by elastic modeling of explosions would be observable under ideal conditions, but detecting an explosion in the m_b5 range would probably be more challenging in practice because of the small area of the deformation field, and would probably require an interferogram with proportionately better coherence. Non-linear and inelastic effects generally act to intensify, but also modify, the deformation produced by shallow explosions, and also need to be considered in interpreting InSAR data.

REFERENCES

Feigl, K.L., A. Sergent, and D. Jacq, Estimation of an earthquake focal mechanism from a satellite radar interferogram: Application to the December 4, 1992 Landers aftershock, Geophys. Res. Let., 22, 1037-1040, 1995.

Massonet, D., M. Rossi, C. Carmona, F. Adragna, G. Peltzer, K. Feigl, and T. Rabaute, The displacement field of the Landers earthquake mapped by radar interferometry, Nature, 369, 227-230, 1997.

Murphy, J., Types of seismic events and their source descriptions, in Monitoring a Comprehensive Test Ban Treaty, editors E. S. Husebye and A. M. Dainty, Kluwer Academic Publishers, Dordrecht, 225-246. 1996.

Okada, Y, Surface deformation due to shear and tensile faults in a half space, Bull. Seismol. Soc. Am., 75, 1135-1154, 1985.

Patton, H.J., and W.R. Walter, Regional moment:magnitude relations for earthquakes and explosions, Geophys. Res. Let., 20, 277-280, 1993.

Patton, H.J., and W.R. Walter, Correction to "Regional moment:magnitude relations for earthquakes and explosions" by Howard J. Patton and William R. Walter, Geophys. Res. Let., 21, 743, 1994.

Pechmann, J.C., W.R. Walter, S.J. Nava, and W.J. Arabasz, The February 3, 1995, M_L5.1 seismic event in the Trona mining district of southwestern Wyoming, Seismol. Res. Let., 66, 25-34, 1995.

U.S. Department of Labor, Mine Safety and Health Administration, Technical investigation report: Fatal mine collapse accident, Solvay mine, Denver Safety and Health technology Center, Denver, CO, 49 p, 1996.

Zebker, H.A., P.A. Rosen, R.M. Goldstein, A. Gabriel, and C.L. Werner, On the derivation of coseismic displacement fields using differential radar interferometry: The Landers earthquake, J. Geophys. Res., 99, 19,617-19,634, 1994.

Acknowledgments

This work was performed under the auspices of the U.S. Department of Energy by Lawrence Livermore National Laboratory under contract No. W-7405-Eng-48 for the Office of Research and Development, NN-20, within the Office of NonProliferation and National Security, NN-1.

FIGURE CAPTIONS

Figure 1: InSAR Geometry

Figure 2: Synthetic surface elastic displacement fields and corresponding interferograms for m_b5.0 events. (a) explosion at 0.3 km depth; (b) earthquake at 2 km depth; (c) mine collapse at 1 km depth. See text for earthquake and collapse source parameters. Surface projections of the earthquake and collapse source planes are shown in (b) and (c). Displacements are projected into the slant range direction for a N-S satellite orbit and 23° look-angle. Displacement contour intervals are 0.01m in (a) and (b), 0.02m from 0.02m to 0.1m and 0.1m thereafter in (c). Each gray cycle in the interferograms corresponds to 2π of differential phase (one fringe).

Figure 3: Synthetic interferograms for: (a) m_b5.2 explosion at 0.3 km depth; (b) M_W5.1 Landers aftershock at 2.6 km depth; (c) M_L5.2 Solvay mine collapse at 0.5 km depth. See text for earthquake and collapse source parameters. Gray scale the same as in Figure 2.

Figure 4: Synthetic elastic vertical surface displacements for m_b5.0 events at different source depths; solid - explosion; dotted - earthquake; dashed - mine collapse. Horizontal bold dashed line indicates displacement detection threshold for C-band SAR 90.028m).

Figure 5: Synthetic elastic vertical surface displacements for m_b5.0 explosion at 0.3 km depth in different elastic media. Dashed - Poisson ratio 0.25, rigidity $3x10^{10}$Nm,; solid - Poisson ratio 0.26, rigidity $1.32x10^{10}$Nm.

Figure 6: (a) Displacement (topography removed) SAR interferogram of the region of the Solvay mine; (b) deformation map obtained by unwrapping the interferogram phase. The 45x33 km area shown is taken from the full 110x100 km scene. The location of the Solvay mine and maximum displacements corresponding to prominent interference patterns are shown in (b). Large black areas at the center and in the NW quadrant of (b) are lakes, which appear as patches of incoherent differential phase in the interferogram.

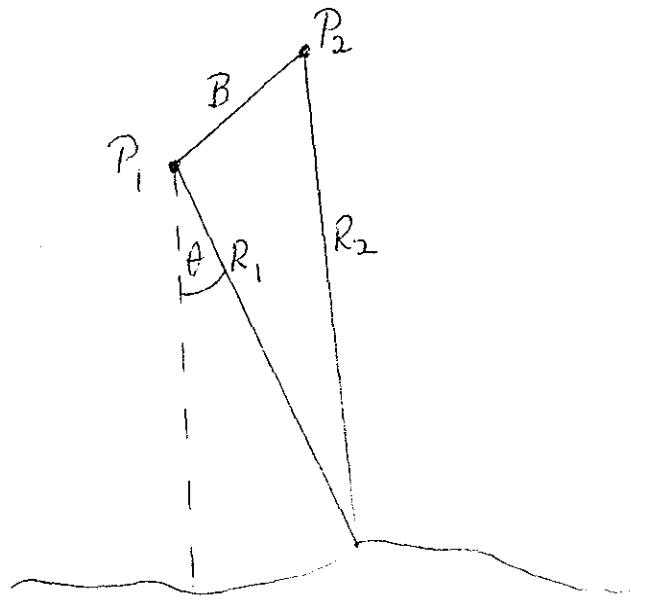

Fig. 1.

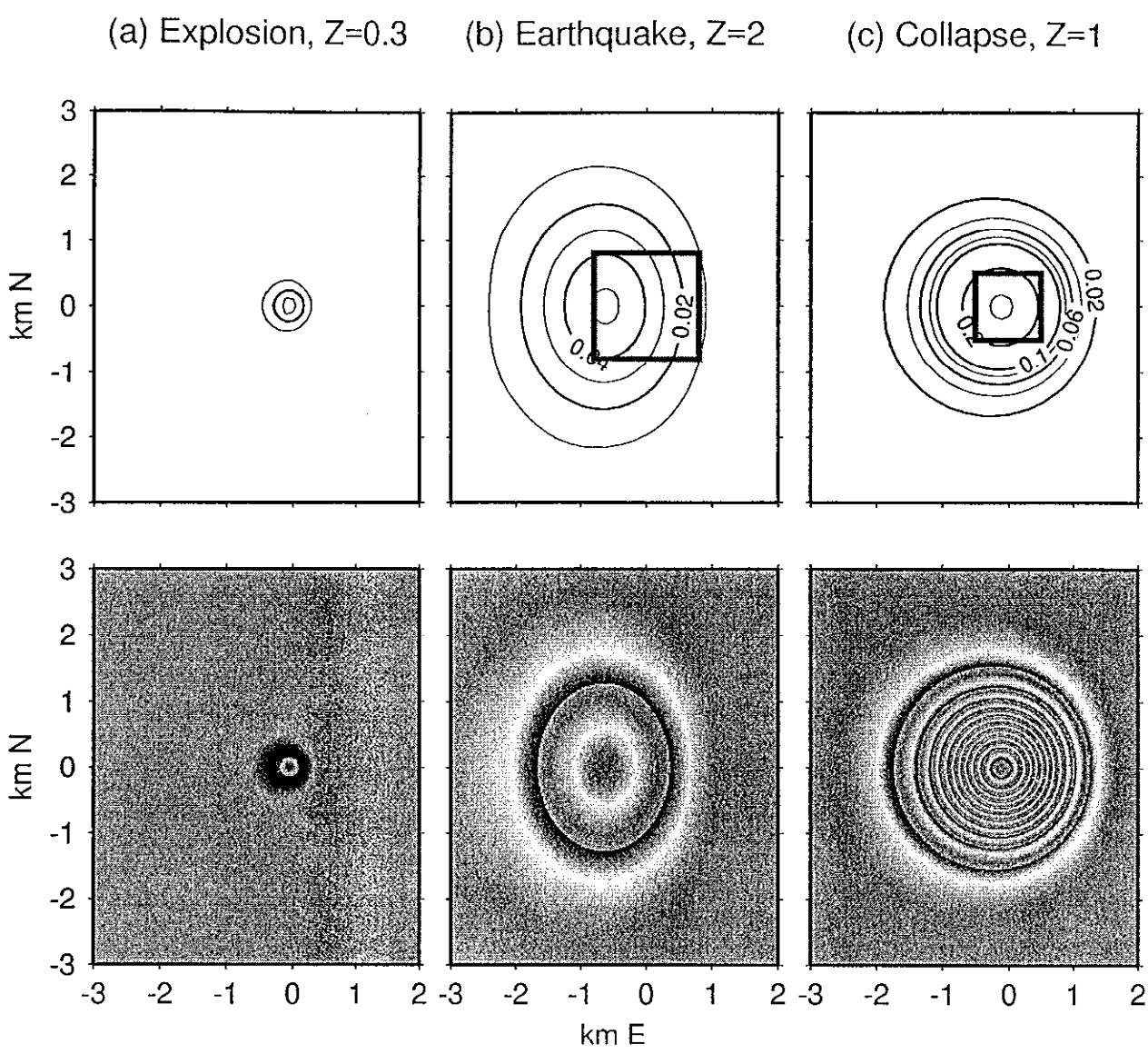
(a) Explosion, Z=0.3
(b) Earthquake, Z=2
(c) Collapse, Z=1
km N
km E
0.02
0.06
0.1
0.2

(a) Explosion, Z=0.3 (b) Landers a/s, z=2.6 (c) Collapse, Z=0.5

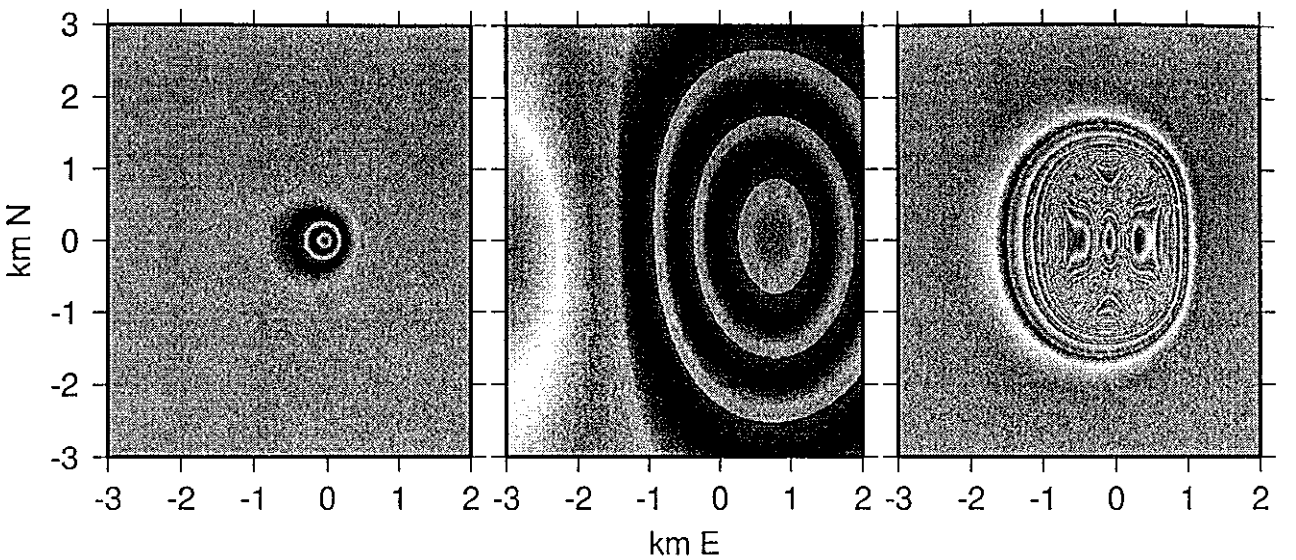

Fig 2

(a)

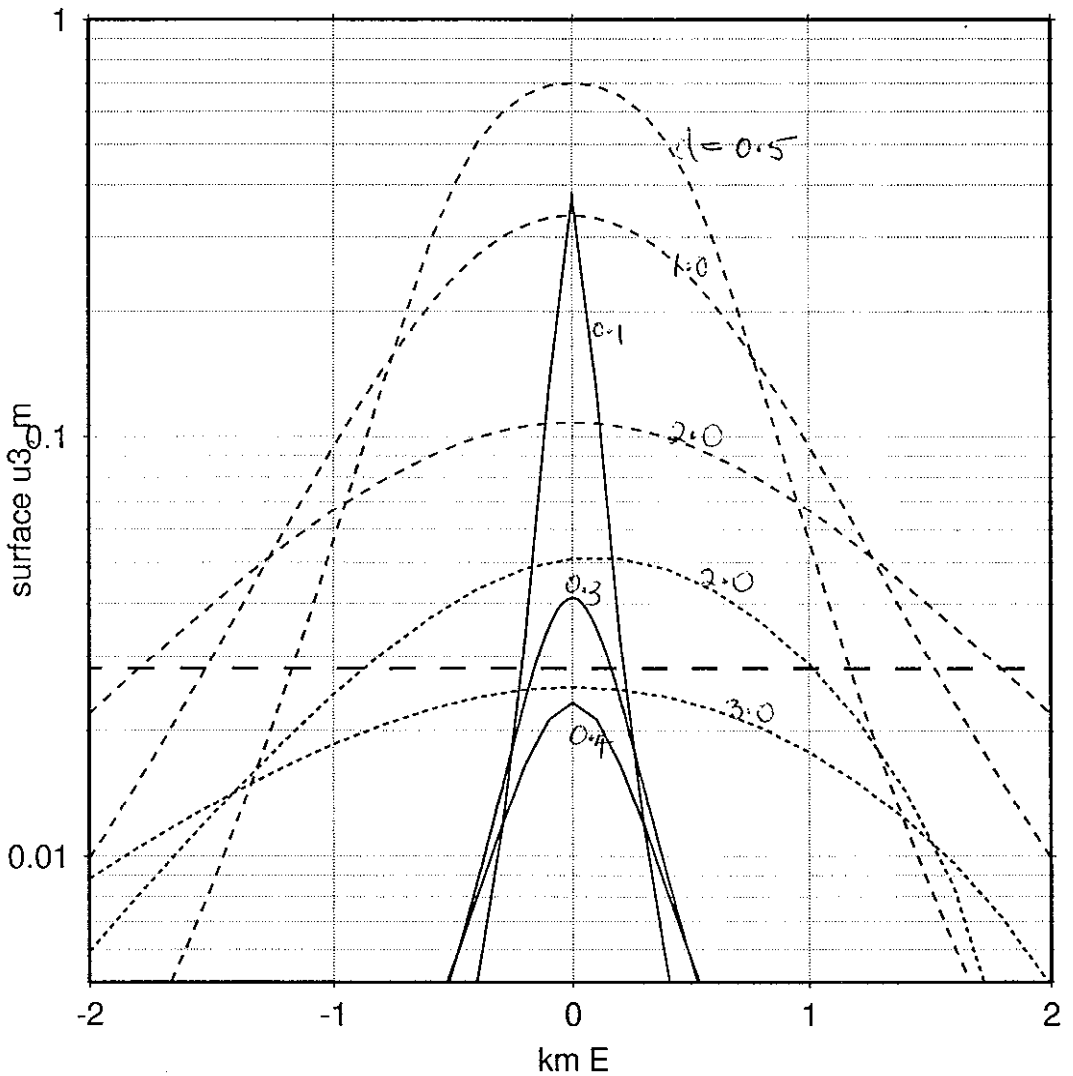

Fig. 11

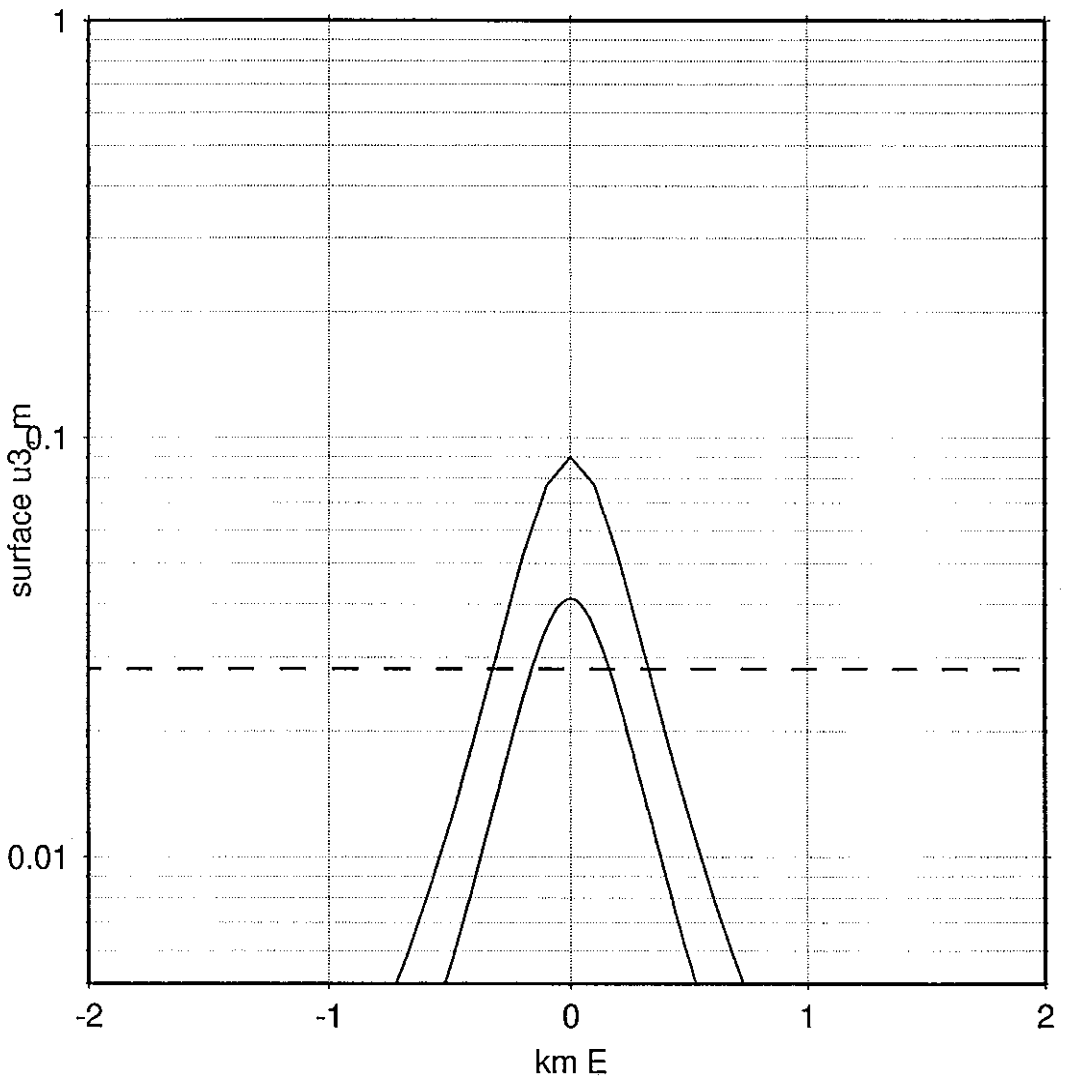
1
0.1
0.01
surface u3_g m
-2
-1
0
1
2
km E

Radar Interferogram

Deformation Map